Journal of Polymer Research (2024) 31:226
https://doi.org/10.1007/s10965-024-04064-7

ORIGINAL PAPER

# Performance of graphene-functionalized nano chitosan in ternary polymeric nanocomposites for physical and biological applications

Sarah Sabah Aljelawy[1,2] · Ehssan Al-Bermany[1] · Ali Razzaq Abdulridha[1]

Received: 31 May 2024 / Accepted: 3 July 2024


## Abstract

Chitosan and vinyl polymer have notably contributed to critical engineering and medical applications. This study focused on combining these biopolymers with the reinforcement of unique graphene to fabricate newly quaternary biopolymers-based nanocomposites for the first time for notable characterizations and properties. The nano chitosan (CS) doped graphene oxide (GO) nanosheet was mixed with two selected vinyl family polymers with different end vinyl functionalities, polyvinyl propylene (PVP) and polyvinyl alcohol (PVA). It was mixed separately with polyacrylic acid (PAA) and CS-doped GO nanosheets to fabricate new PVP-PAA-CS/GO (Ps) and PVV-PAA-CS/GO (Ns) nanocomposites. Fourier-transform infrared spectroscopy exhibited strong hydrogen bonding between the component matrix with different behaviors of nanocomposites. X-ray diffraction results revealed different semicrystalline behavior of nanocomposites due to changing the vinyl polymers. Field emission scanning electron microscopy presented good homogeneity and fine dispersion of nanomaterials with different fracture surface behavior of two nanocomposites. UV–visible spectrophotometer utilized absorption peaks at 260 nm of Ps and 300 nm of Ns nanocomposites; the energy gap improved the forbidden indirect transition from 3.4 to 2.95 eV and 3.9 to 3.2 eV, respectively. The inhibition zone of bacteria presented the best result of Ps nanocomposites, which improved from 6.2 mm to 14 mm *S. aureus* bacteria ranged, whereas 7 mm to 11 mm was the range for group Ns. Meanwhile, Ps revealed the best inhibitory of *E. coli* from 19 to 23 mm and 18 to 20 mm for Ns nanocomposites compared to *S. aureus*. These new nanocomposites presented promising for biological and opto-electro applications.

**Keywords** PVA · PVP · CS · GO · Optical · Antibacterial

## Introduction

Polymer blends are widely acknowledged across various industrial sectors for their varied and advantageous properties. The utilization of blended polymers has been explored to attain novel matrix characteristics [1]. These blended polymers offer numerous advantages, such as improved mechanical, thermal, electrical, structural, and optical qualities [2]. The optical characteristics of composite thin films comprising solid dielectric materials like polymers or glass offer innovative applications in photo-electronic devices, leveraging quantum-sized belongings [3, 4].

An interesting Vinyl group of polymers derived from substituted vinyl ($H_2C=CHR$) monomers. It has a composed backbone consisting of a lengthy alkane chain [$-CH_2-CHR-$] [5]. Because of the vinyl polymer's characterizations, it has become more attractive to researchers and engineers for a wide spread of applications. Polyvinyl alcohol (PVA) and polyvinyl pyrrolidone (PVP) are the most exciting polymers with hydrophilic properties and biocompatibility. It is associated with several essential applications, such as industrial and medical applications [1, 6]. Where PVP could form hydrogen bonds associated with increasing the melting points, it can improve the stability of blends in physiological situations and display superior complex features. Whereas PVA is a semi-crystalline polymer and excellent binder that makes it required and useable in several applications by industrial and scientists [7]. Where PVA and PVP can stop particle aggregation by electric repulsion and have hydroxyl and carbonyl groups that make a strong binding with other polymers [8, 9].

✉ Ehssan Al-Bermany
ehssan@uobabylon.edu.iq

[1] Physics Department, College of Education for Pure Sciences, University of Babylon, Babylon, Iraq

[2] Physics Department, College of Science, University of Babylon, Babylon, Iraq

Published online: 15 July 2024

Polyacrylic acid (PAA) is a further example, where each monomer unit has a carboxylic group. When the polymer comes into contact with water, these acid groups separate, and the polymer becomes a polyelectrolyte [10]. Polyacrylic acids (PAA) are non-toxic and widely used to increase water viscosity, which thickens solutions. They have many advantages. Due to its gel-like structure and high-water absorption capacity, this chemical compound finds extensive use in various sectors, including producing soft contact lenses. Soft tissue creation, artificial cornea fields, oil recovery, surface grafting polymerization, flocculants, and water and mining treatment for burn coverage are more uses [11, 12].

The presence of amino groups within the chitosan (CS) structure enables protonation, imparting solubility in aqueous solutions with diluted acids. Chitosan possesses numerous noteworthy properties that provide unique opportunities for advancing applications in biomedicine. Its hemostatic activity can be attributed to the positive charges present on the chitosan backbone. These positive charges facilitate interactions with the negatively charged regions of cell membranes, leading to the tight junction protein rearrangement and opening, thereby elucidating its feature that enhances penetration. Additionally, the chitosan's polycationic properties offer insights into its analgesic effects. Regarding chitosan's biodegradability, it's essential to note that chitosan is more than just a polymer containing, in addition to amino groups, a polysaccharide, thus featuring breakable linkages in glycosidic. In vivo, chitosan undergoes degradation primarily by various proteases, particularly lysozyme [13]. Due to its biocompatibility, biodegradability, and non-toxic nature, chitosan finds applications in medical settings as antimicrobial agents and healing wound biomaterials. Furthermore, its chelating ability, allowing it to attach itself to proteins, lipids, cholesterol, and metal ions, enhances its utility as a chelating agent [14]. Chitosan, its derivatives, and Chito oligosaccharides demonstrate antimicrobial effects against various microorganisms, encompassing bacteria, filamentous fungi, and yeast [15]. Chitosan appears to possess growth-inhibiting properties, as bacteria can increase once the polymer is removed from the medium. This observation is significant as it suggests the potential emergence of resistant populations if cells adapt to chitosan over time [16].

Incorporating a small percentage of nanoparticles into the polymer matrix could influence the structure and properties of the matrix [17]. As per an exciting nanomaterial suggested framework [18], graphene oxide nanosheets (GO) consist of flat graphene, similar to aromatic regions. This has various sizes connected by a cyclohexane network as units arranged in a chair shape. These regions are decorated with functional groups, such as hydroxyl, ether, ketone, epoxy, and diol. The lack of these functional groups could cause aggregation and precipitation because they give the individual sheets their water solubility [19]. Despite being electrically insulating in its heavily oxidized state, the nanosheets could restore the conductivity via thermal or chemical produces. Most graphene oxide is produced using Hummers and Offerman's process [20]. This will create vast opportunities to leverage the unique properties of graphene for numerous technological applications. Graphene oxide (GO) with increased reactivity can effectively interact with cells, readily coating cell surfaces and exhibiting a greater affinity for bacteria. Its sharp edges and exceptional mechanical strength suggest that GO may act as "nano-knives," potentially damaging cell membranes [21]. GO suspensions are toxic to bacteria, displaying significant antibacterial activity, particularly against Gram-positive compared to Gram-negative bacteria. The attachment of bacterial cells to GO or GO-coated surfaces has been observed to disrupt cell integrity and decrease cell viability, hindering bacterial growth. Reported toxicity mechanisms of GO against microorganisms include oxidative stress induction, microbial entrapment within GO nanosheets, GO's sharp edges damaging the cell membrane, and electron transfer interaction between the microbial membranes with GO nanosheets [22, 23]. The global issue of bacterial resistance to antibiotics has emerged, with bacteria developing resistance even against third-generation antibiotics [24].

In contrast, Abou-Taleb's [25] study explored alterations in the optical properties of augmentation of PVA with PVP with different ratios. They illustrated the crystalline characteristics and absorption behavior. The finding is attributed to the interaction between the polymers via the carbonyl and hydroxyl groups. This investigation was conducted by Hatta et al.[26] A PVA: PVP was synthesized using various ratios, where 80% of PVA showed the highest electrical conductivity. To consider the issue more, the spotlight was on nano metal composites containing Au or Ag that improved the optical properties of their samples [10]. PVP was mixed with the europium ethylenediamine tetraacetic acid (Eu EDTA) doped with Ag. It exhibited significant fluorescence activity. Additionally, it presented interesting materials for various industry applications, such as light-emitting diodes (LEDs), laser materials, biosensors, and assay development [27]. Other researchers [28] reported fabricated PVA: PVP bled polymer with a ratio of (1:1). It was loaded with LiBr and $Ag_{1.6}Cu_{0.2}S$ (ACS) with different ratios (0.1, 0.5, 1.0, 5.0, and 10 wt.%) for potential technical applications. Where the contribution of doped ACS into PVP: PVA exhibited a significantly decreased optical bandgap from 5.21/4.95 eV of ($PVP/PVA_0$) to 4.87/4.54 eV of ($PVP/PVA_{10}$) for the direct/indirect energy gap, respectively. Furthermore, significant enhancements in both linear and nonlinear optical parameters were observed after the contribution of ACS. The dielectric constants increased from 2.87 to 3.63, and a two-order increase in nonlinear third-order susceptibility with 10% ACS doping ($PVP/PVA_{10}$), indicating significant

improvement in magnetite enhancement. Ming Yang [29] explores the synthesis of PVA hydrogel techniques by incorporating various bio-additives to enhance biocompatibility and bio-hydrogels for application across diverse lines. Illustrative instances are meticulously chosen and deliberated upon, considering their composition and advantages and disadvantages. In a separate investigation conducted by Zein K. Heiba et al., a PVA: PVP doped varying ratios of nano $Cu_{0.9}Mn_{0.1}S$ (Cu/MnS) were infused using thermolysis and casting techniques. The incorporation of Cu/MnS led to a notable decrease in the PVA/PVP bandgap, which could be adjusted depending on the doping level. The real dielectric constant and imaginary components also increased with higher amounts of Cu/MnS doping. [30].

Several investigations [25, 29, 30] deal with the impact of functional nanofiller gropes on the polymers' properties. This study's first aim focused on comparing the effect of two different functional groups of two polymers from the vinyl family to understand the impact of vinyl groups on the final results. Meanwhile, the second aim is to investigate the impact of loading nano chitosan polymer functionalized with GO in independent PVP- and PVA-based nanocomposites. Therefore, several samples were fabricated as two groups of nanocomposites: first, was PVP blended with PAA and CS, then reinforced with GO nanosheets to prepare PVP-PAA-CS/GO nanocomposite, and second fabricated PVA-PAA-CS/GO in for the first time the form of a film. Different methods and characterizations were utilized to investigate these novel nanocomposites, such as Fourier-transform infrared spectroscopy (FTIR), X-ray diffraction (XRD), Field emission scanning electron microscopy (FESEM), and UV–visible spectrophotometer, and two positive and negative bacterial types for antibacterial activity.

## The Experimental Part

### Materials

PVA with the chemical formula $(C_2H_4O)n$ with a molecular weight (Mw) of (115,000) $g.mol^{-1}$ was provided by Dindori company, India. PVP Mw's is (40.000) $g.mol^{-1}$ with chemical formula $(C_6H_9NO)n$, brought from Alpha Chemical Company, India. PAA with the chemical formula $(C_3H_5NO)$ n and molecular weight (71.07) $g.mol^{-1}$ for each molecule provided by Wuxi Lansen Chemicals company, China. Chitosan (CS) (nano polymer) has Mw of (161) $g.mol^{-1}$ chemical formula $(C_6H_{11}NO_4)n$, white or off-white powder, specific gravity (1.4) that is made in Canada. Graphene oxide (GO) is synthesized following the methodology outlined in our prior publication [31].

### Formulations and mixing of samples

The preparation of samples was divided into three steps, as briefly explained below.

Step 1: All polymers were dissolved in distilled water before mixing at 9 g in 50 ml. Then, the mixing ratio of PVA and PAA was (50:50) wt.% to prepare the first group of model blend polymers (N1). Meanwhile, the same ratio was utilized to prepare the second group of blended polymers by mixing PVP and PAA to prepare (P1) groups.

Step 2: To prepare both (N2) and (P2), the ratio of PVA was kept at 50 wt.%, whereas the ratio of PAA was changed to 25 wt.% within the addition of 25 wt.% of polymer CS. The same procedure was applied to (P2).

Step 3: To fabricate the new nanocomposites, a ratio of 2 wt.% of graphene oxide was added, which was considered the effective ratio in some research for both groups separately.

The specimens were transferred into Petri dishes, which dried for five days under air at abundant temperature. Table 1 and Fig. 1 show the above steps of the formulation of samples.

### Characterizations

The FTIR analysis within the 4000 –400 $cm^{-1}$ was conducted using a Vertex 70 spectrometer from a Bruker. XRD was performed using PW1730, Philips Company, USA. A Tuscan company in the Czech Republic introduced FESEM type TESCAN Mira3. The optical properties were recorded using a double beam UV–visible spectrophotometer,

**Table 1** Percentages of mixing weight of the sample

| Sample ID | Concentration wt. % | | | | |
|---|---|---|---|---|---|
| | PVA | PVP | PAA | CS | GO |
| **N1** | 50 | - | 50 | - | - |
| **N2** | 50 | - | 25 | 25 | - |
| **N3** | 50 | - | 24 | 24 | 2 |
| **P1** | - | 50 | 50 | - | - |
| **P2** | - | 50 | 25 | 25 | - |
| **P3** | - | 50 | 24 | 24 | 2 |

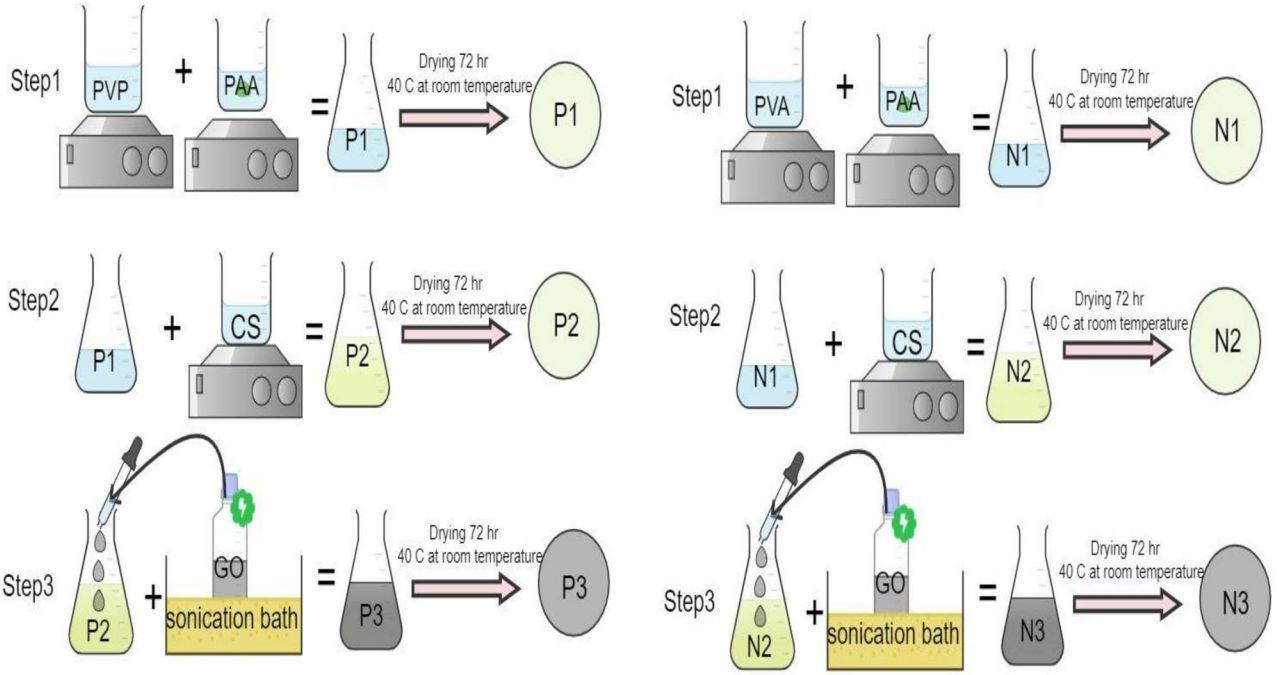


**Fig. 1** Diagram outlining the experimental procedures for fabricating sample films

specifically, the Vertex 701, 190–1100 nm wavelength made by Phillips Company, Japan.

## Results and discussion

For groups Ps and Ns, respectively, the FT-IR spectra of the P1, N1, P2, N2, and P3, N3 samples were recorded in areas between (4000- 600 $cm^{-1}$) (RT), as illustrated in Fig. 2(a and b). The spectra for the two polymers' combined molecular vibration patterns in the Ps group are displayed in Fig. (2a). P1 appeared peaks at 3414, 2921, 2823, 1620, 1531, 1419, 1287, 1184, and 816 $cm^{-1}$ associated to (O–H) stretch, methylene (C-$H_2$) stretching aliphatic group (C = C) unsaturated compounds at (C–C) stretch bands within ring skeleton bend and carbon dioxide (C-O), inorganic carbonate (C = O) stretching, epoxy group (C–O–C) and CH out of plane aromatic band, respectively [32]. Slight shifting presented of these peaks of P2 from 3344, 2922, 2852, 2358, 1720, 1646, 1491, 1285, 1069, and 797 $cm^{-1}$, meanwhile new peaks presented at 2358 and 1069 $cm^{-1}$ associated with 2355 and 1066 $cm^{-1}$ respectively, that presented as a result of adding a CS polymer. The contribution of GO nanosheets in P3 revealed the changes in the intensity of 3291, 1641, and 798 $cm^{-1}$ peaks and presented the peaks at 1700 and 1400 $cm^{-1}$. The finding of PAA-PVA/GO showed minimal shifts in most broad peaks following the inclusion of CS and GO nanosheets, consistent with another observation [33].

A broadband peak of 3285, 2940, 1715, and 1087 $cm^{-1}$ was seen in Fig. 2b of the PAA-PVA (N1) spectrum. This peak was linked to the increased oscillations of the amide group, (O–H) hydroxyl group, (C-H) methylene, stretch (C = O) carboxyl acid, and (C–O–C) epoxy group. The hydroxyl (OH), methylene (C-H), C-N stretching, carboxylic acid (C = O) extended, amide group, hydroxyl group (OH), and epoxy group (C–O–C) expansion oscillations were linked to the peak range in N2 at 3244, 2923, 1703, 1608, 1414, 1061, and 831 $cm^{-1}$, in agreement with literature [34].

The molecular vibration patterns shape analysis of PAA-PVA/GO (N3) revealed identical peaks to those of the polymer, albeit with shifted positions following the inclusion of GO nanosheets, corroborating findings from another study [33]. Changes in the locations of the peaks, or the disappearance of some of them and the appearance of new ones, indicate a strong bond between the materials. A strong hydrogen bond may be the most common among the materials with GO nanosheets, as agreed by researchers [2]. The results showed that the peaks of the Ps group were different in the area between 3291 to 600 $cm^{-1}$ compared with those of the Ns group. Table 2 summarizes some of the FTIR functional groups presented with matching literature reviews.

Figures 3(a and b) show the XRD spectra of samples. The PVP and PAA (P1) mixture presented a semicrystalline behavior with an abroad peak between 10° to 35°. The top of the abroad peak at 20°, which related to combining both polymers with small features at 13.4° that could relate to

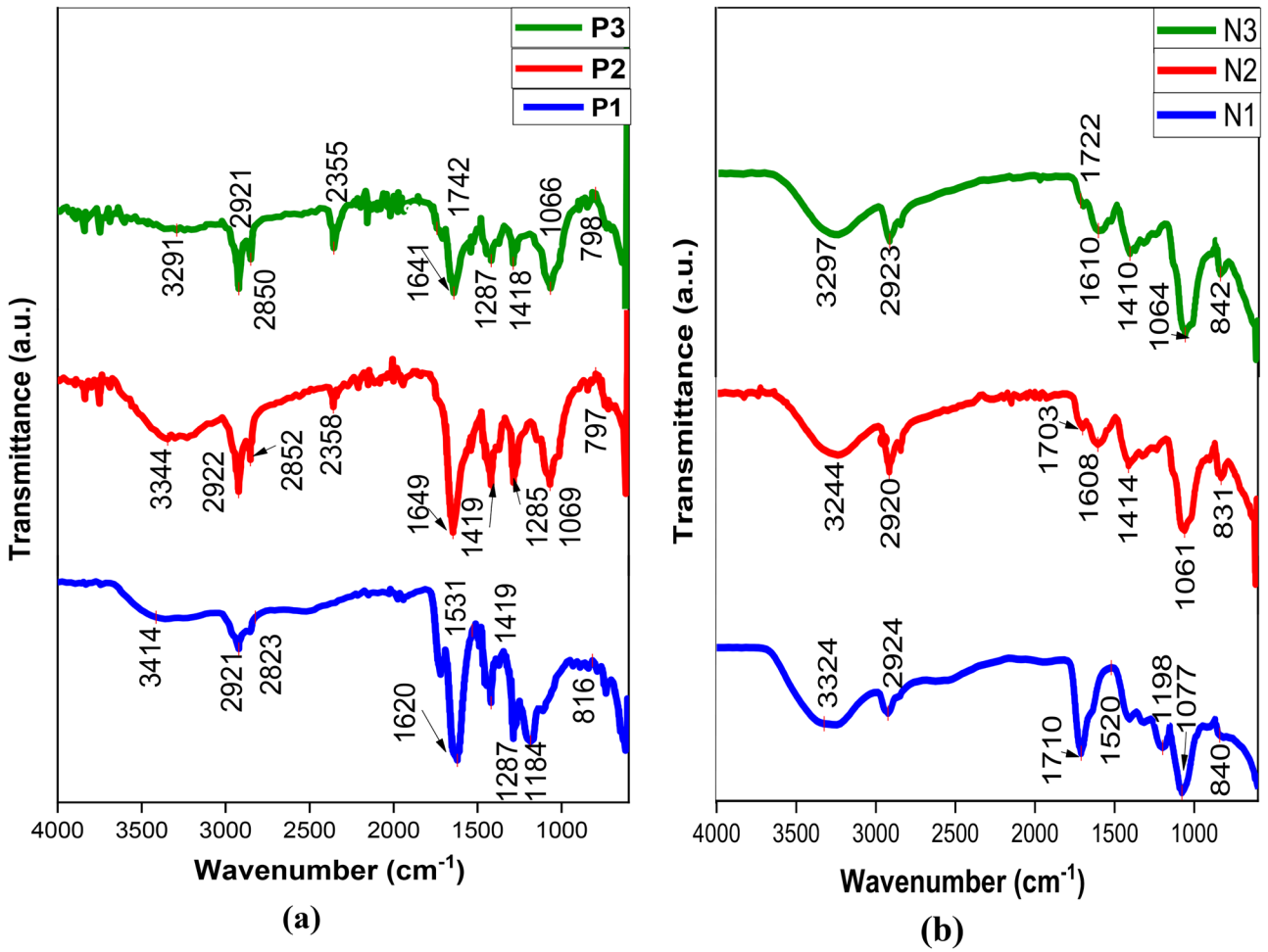


**Fig. 2** FTIR spectra of samples **a** (PVP-PAA, PVP-PAA-CS, and PVP-PAA-CS/GO), **b** (PVA-PAA, PVA-PAA-CS, and PVA-PAA-CS/GO)

PVP; these results matched another finding [2, 49]. CS was added to a mixture of P1 to fabricated P2; peaks appeared at 13 and abroad between 11.1 ° and 30.55°. The top of the abroad peak at 23.7°. These new peaks were attributed to the addition of CS in agreement with the literature [49, 50]. The results clearly showed peaks of chitosan when compared with the blended polymer (P1). Meanwhile, the contribution of graphene oxide is clearly presented in P3 in

**Table 2** Summarizes some of the FTIR functional groups presented with matching literature reviews

| Peak, $cm^{-1}$ | Functional groups | | | References |
|---|---|---|---|---|
| | Group | Class | Peak Details | |
| **3414—3297** | O–H stretching | alcohol | strong, broad | [32, 35–37] |
| **2924—2824** | C-H stretching | alkane | Medium—weak | [35, 37, 38] |
| **2358** | O = C = O stretching | carbon dioxide | strong | [34, 39] |
| **1710** | C = O stretching | carboxylic acid | strong | [40, 41] |
| **1620** | C = C stretching | α, βunsaturated ketone | strong | [42, 43] |
| **1520** | C–O–C stretching | epoxy group | strong | [21, 37] |
| **1419** | O–H bending | alcohol | medium | [21, 40] |
| **1287** | C-O stretching | aromatic ester | Strong | [32, 44] |
| **1198** | C-N stretching | amine | medium | [45, 46] |
| **1184** | C-O stretching | ester | strong | [32, 47] |
| **1077** | C-O stretching | primary alcohol | strong | [44, 48] |
| **840–816** | C = C bending | alkene | medium | [32, 35] |

Fig. 3 a, where a clear GO peak is presented at 10.7°. The distance between the planes (d) is 7.5 Å, whereas an abroad diffraction peak becomes between 20.55° to 34.35° compared with P1 and P2. The expansion of interlayer spacing in graphene oxide is attributed to the presence of oxygen functional groups and water molecules within the carbon layer structure. These represent common vertical oxides of graphene [32].

In Fig. 3(b), it is noticeable that the different peaks and behavior of Ns compared with Ps result from the base PVP polymer, which became PVA. The X-ray diffraction profile of PVA-PAA (N1) and related groups of nanocomposite powder is shown in Fig. 3(b). The crystalline solid reflection peak presented at $2\Theta = 19.75^{\circ}$ represents reflections from (101) from a monoclinic unit cell [51], which is 25 related to PVA in agreement with the literature [52]. Other minor features of peaks presented at 23.65°and 40.10°. This diffraction pattern corresponds to the atactic trans-planar conformation of PVA [52]. Instead, they showed a relatively broad peak at 22.65°, as depicted in Fig. 3(b). A small PVA nanocrystalline phase may co-coexist with the bulk amorphous phase based on the minimal degree of crystallinity and significant diffuse scattering observed in this PVA diffraction pattern.

In N2 composed of PVA-PAA-CS, the peaks were observed at 19.7°, 22.8°, and 41.4°. The appearance of peaks at 19.7° and 41.4° can be attributed to CS, consistent with existing literature [53], and the peaks at 22.8° coincide with N1, which appeared at 23.65°. The contribution of GO, a peak appeared at 10.25° that attributed to GO in stronger agreement with the literature [54], while the peaks shifted from 19.7 to 18.35◦ and from 22.8 to 20.45°, whereas other small features or peaks presented at 26.7° and, 32.6°, 35.6° and 48.6°. These results strongly agreed with the FTIR finding that revealed strong interfacial interactions, as reported in other findings [55].

Using FESEM for Ps and Ns samples, the dispersion of the nanomaterials in the matrix and the surface morphology of the samples were inspected. as exposed in Figs. 4 and 5, respectively. The left side was at a magnification of 10 µm, whereas the right side was at a magnification of 500 nm of the same sample. Figure 4 shows the FESEM images of P1, P2, and P3 blend polymers. These images showed the

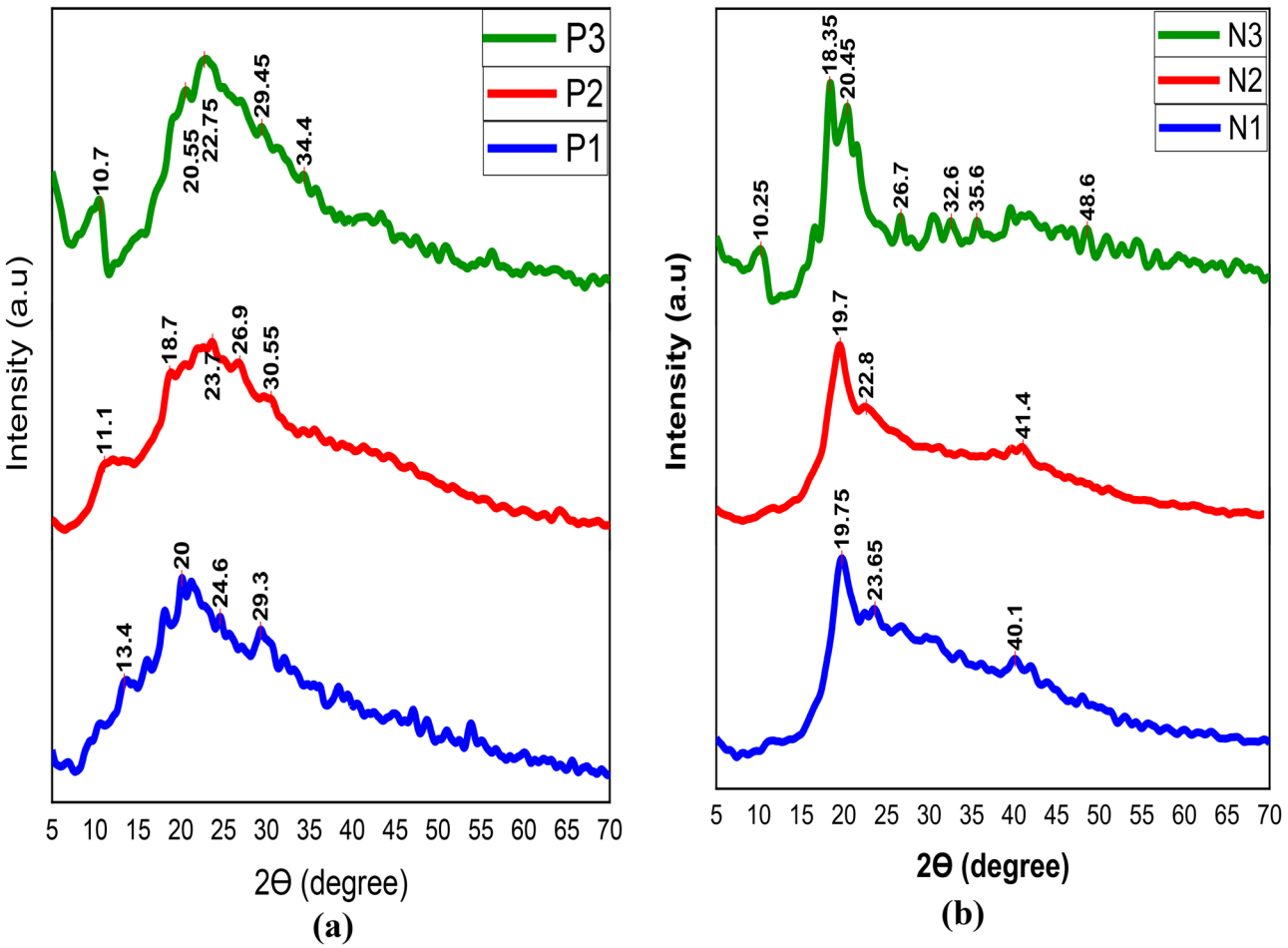


**Fig. 3** The XRD patterns of **a** (PVP-PAA, PVP-PAA-CS, and PVP-PAA-CS/GO), **b** (PVA-PAA, PVA-PAA-CS, and PVA-PAA-CS/GO)

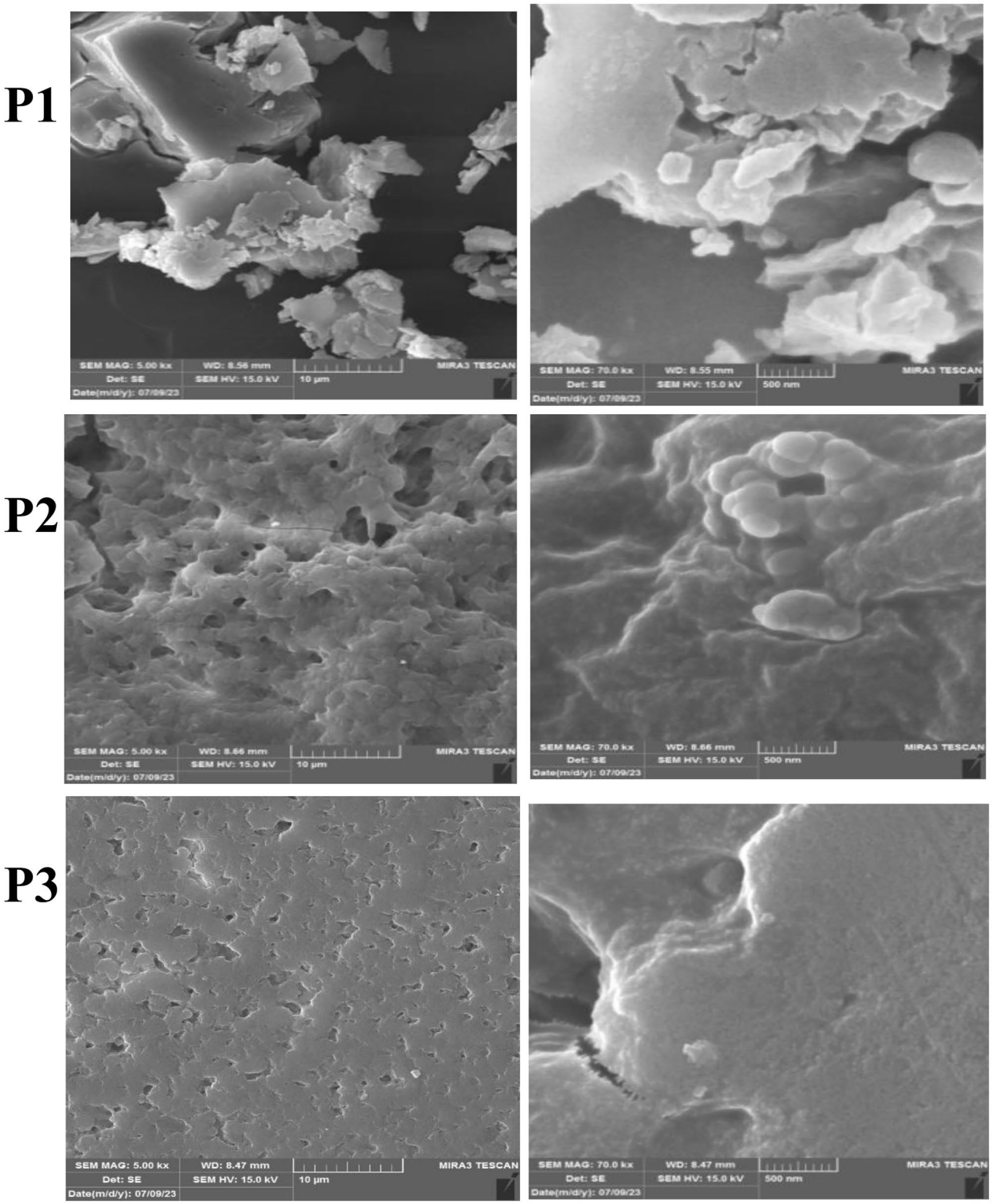


**Fig. 4** FESEM images for P1, P2, and P3 samples

density and flaky surface of P1. The P2 revealed a change in surface morphology behavior with good bonding and adhesions between the blended polymers. These polymers were significantly enhanced by adding graphene oxide in the P3. GO The nanosheets exhibited favorable dispersion with a granular structure, appearing without aggregations. As depicted in Fig. 5, the surface displayed roughness and coarseness, with cracks apparent in both N1 and N2. Interestingly, in N3, the cracks on the surface were notably diminished, becoming less discernible and smoother than the other samples. This improvement can be attributed to the incorporation of GO into the N3 matrix.

Figures 6(a and b) display the optical absorbance behavior in the ultraviolet region ranging (260- 900 nm) of Ps and Ns samples, respectively. This figure indicated a different range. The Optical transitions are observed at the fundamental edge of both

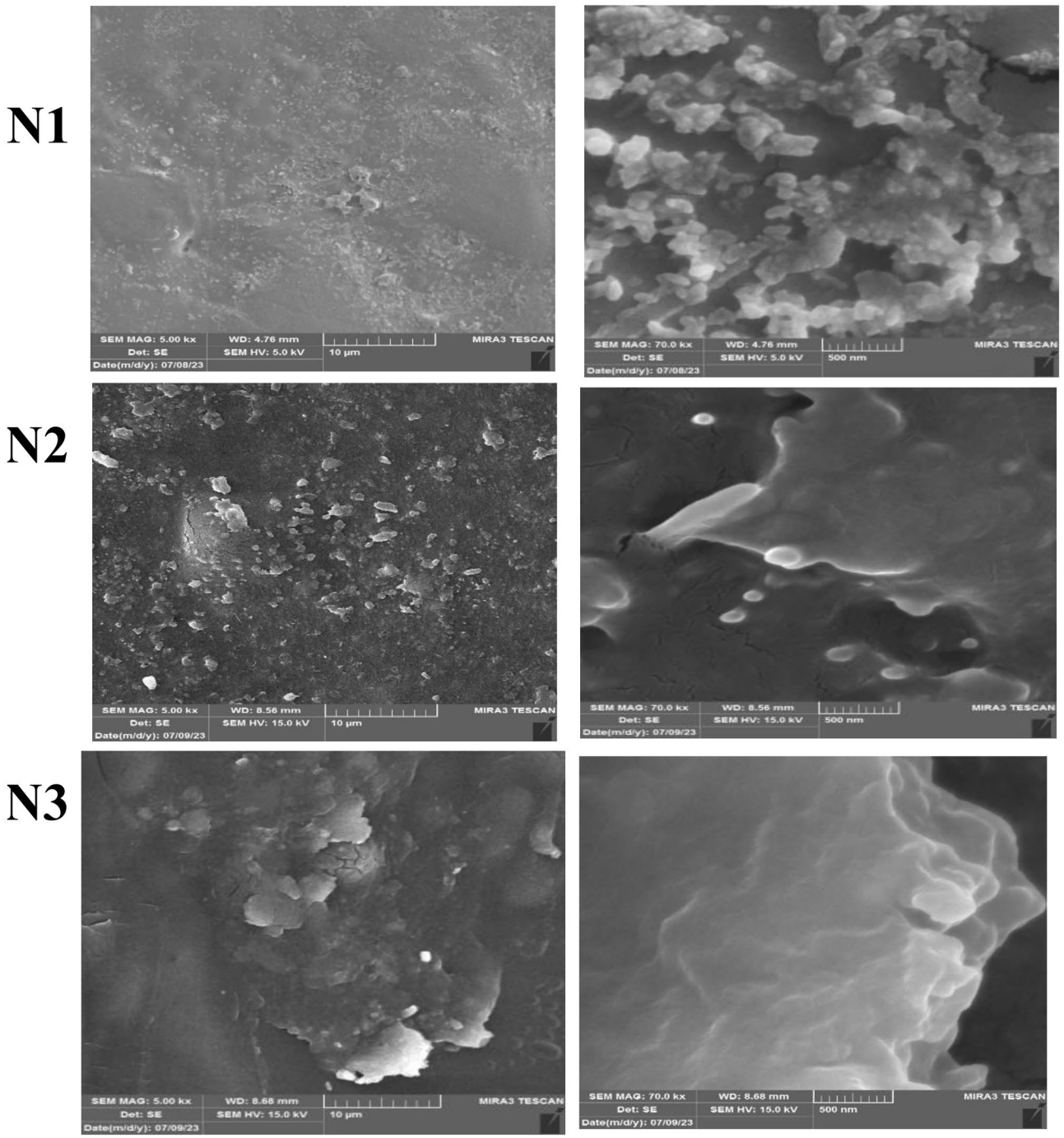


**Fig. 5** FESEM images for N1, N2, and N3 samples

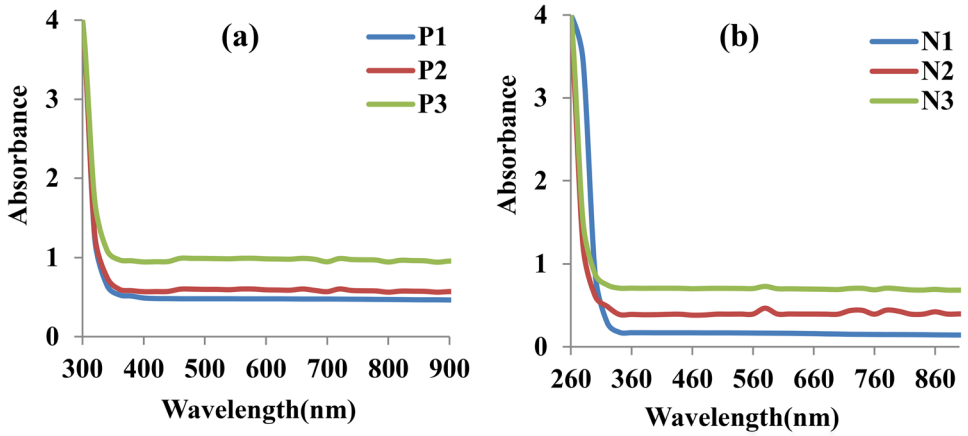


**Fig. 6** The absorbance spectra with the wavelength of samples

crystalline and non-crystalline materials, encompassing both direct and indirect transitions. This occurs within high-absorption regions. The Ps groups exhibited a peak at 300 nm, attributed to transitions involving π-π* stacking transitions and the related correlation arising from interactions between nanomaterials and blended polymers matrix. Conversely, the Ns groups showed absorbance at 260 nm, where electrons from donor levels were excited to the conduction band upon absorbing photons of specific energy, transitioning from lower to higher energy states. Additionally, the results demonstrated the samples' significant absorption of photons in the UV region, providing sufficient energy for interaction with atoms. The fundamental absorption indicates excitation transitions or bands, enabling the study of potential electron transitions through changes in transmission and absorption [56].

Furthermore, the absorbance was boosted by the proportion of CS, while GO nanosheets exhibited the most significant enhancement in the region beyond 300 nm. Remarkably, the incorporation of GO nanosheets led to higher photon absorption compared to other samples in both groups. They demonstrate high absorbance for each nanoflake and can capture up to 2.3% of light across a wide range of wavelengths, rendering them suitable for specific optoelectronic devices and applications [57]. GO nanosheets enhance the incident light absorption through their free electrons. It facilitates interaction between materials and incident photons. The rise in nanosheets abundant with a finely distributed dispersion within the matrix increased the number of charge carriers [58], which aligns with the findings and outcomes documented in the literature [59]. Strong hydrogen bond interactions have been observed between the polymer and GO nanosheets due to GO's abundant chemically reactive sites with free energy in polymer chains. The hydrogen bond is another element thought to contribute to the nanocomposites' increased absorption [60]. The nanocomposite exhibited low absorbance in the visible region, suggesting that incident photons may lack sufficient energy to act with atoms at longer wavelengths, resulting in photon transmission.

The relationship between the materials' incident and absorbed light intensities.

It can be characterized as the absorbance (A) found in Eq. (1) [61].

$$A = \log T \tag{1}$$

where (T) transmittance.

Figures 7 and 8 indicate that rapidly increased transmittance for each sample increases as the wavelength rises. This increase peaked at 260 and 300 nm in the Ps and Ns groups. The results clearly demonstrated how both CS contributed to

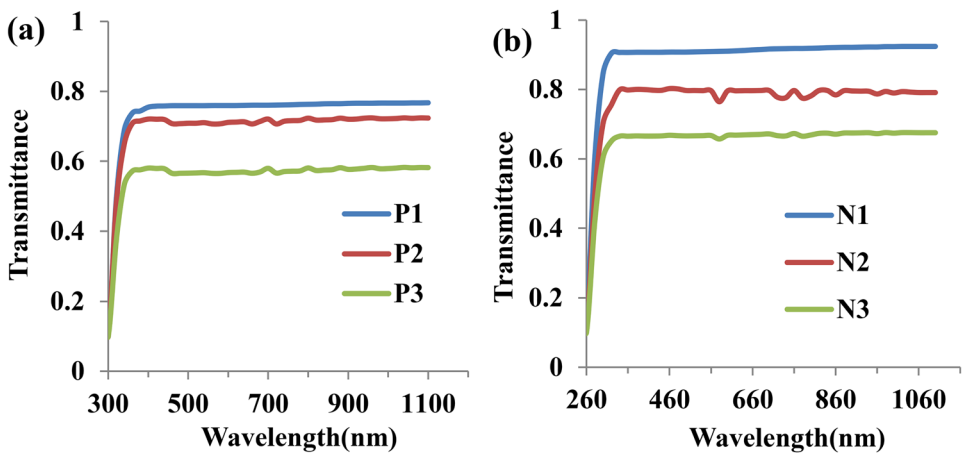


**Fig. 7** The transmittance spectrum has a wavelength of N1, N2, P1, P2, and N3.P3 nanocomposite

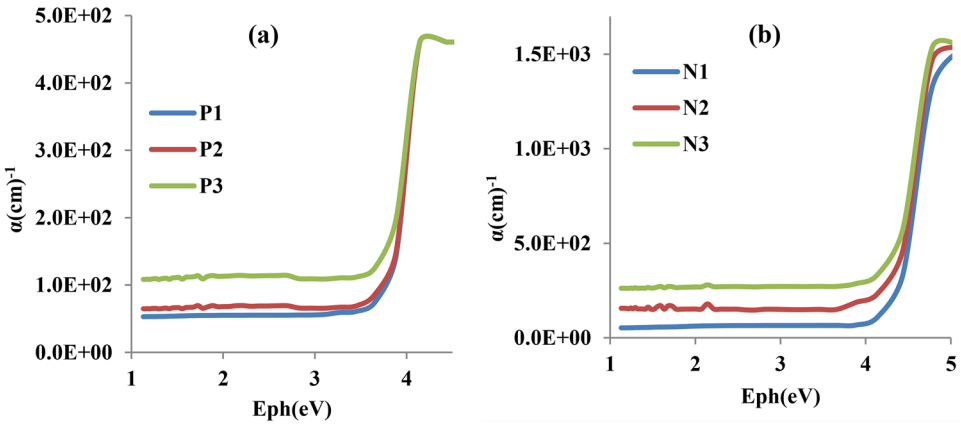


**Fig. 8** The variation of the absorption coefficient with the incident photon energy of the samples

the decrease in light transmittance. Graphene oxide (GO) in the matrix revealed a notably amplified effect, as more nanomaterials could enhance light absorbance and diminish transmission for similar reasons. When comparing the contribution of CS and GO to N1 and N2, the outcomes indicated a drop in transmittance of up to 5.5% and 33% for P1 and P3 and 15% and 35% for N2 and N3 at 800 nm. Notably, the data showed that Ns groups transmitted lighter than Ps groups.

One can determine the absorption coefficient ($\alpha$) using the Lambert-Bear formula [32].

$$\alpha = 2.303\ \frac{A}{t} \tag{2}$$

t is the thickness of the samples.

Figure 9 illustrates the absorption coefficient of sample films. It consistently increases with growing photon energy pending to reaching approximately 3.2 eV. This performance may be related to the lower transition of electrons, where the energy of an incident photon is insufficient to move electrons from the valence to conduction bands. However, beyond 3.2 eV, all samples have a sharp rise in the absorption coefficient due to significant electron transitions to the conductive band. At 3.65 eV, there is a rapid increase in the absorption coefficient, indicating intense electron interaction transmission. Generally, the finding revealed significant enhancement with the contribution of CS and GO in the nanocomposites.

The allowed and forbidden indirect optical energy gaps of samples were computed using formula 3, which determines the interception of the extrapolated linear segment adjacent to the photon energy [62].

$$\alpha h\upsilon = B(h_\upsilon - E_g)^r \tag{3}$$

where formula (3) depends on the transition type, $h_\upsilon$ is photon energy, $E_g$ is the energy gap, ($B$) is constant, and ($r$) represents the exponential constant, $r=2$ and 3 to direct or indirect transitions. Figs. 9 and 10 depict the absorption edge of permitted indirect transitions for Ps and Ns, respectively, about photon energy. The intersection of the linear extrapolation portion was utilized to determine the values at ($E_{g.}$) at this value; the energy gap was computed by sketching a straight line from the higher section of the curve in Figs. 9

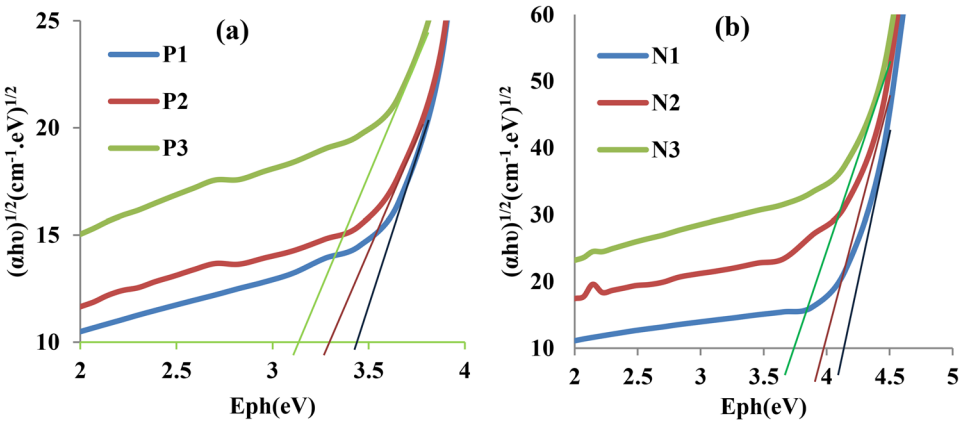


**Fig. 9** The optical energy gap allowed indirect transition with photon energy for the N1, N2, and N3 nanocomposites

and 10 to the x-axis for the permitted indirect transition. In the case of Ps, as shown in Fig. 10a, there was a notable enhancement in the energy gap results of the permitted and prohibited indirect transitions following the inclusion of CS and GO in the sample (P3), increasing by up to 9.5% and 12% respectively compared to P1.

The findings revealed reductions in the energy gap for both allowed and forbidden indirect transitions within the Ps groups, decreasing from 3.45 to 3.05 eV and 3.4 to 2.95 eV, respectively. Conversely, improvements were observed in the Ns group, with the energy gap decreasing from 4.05 to 3.65 eV for permitted transitions and 3.9 to 3.2 eV for prohibited transitions. This indicates enhancements of up to 10% and 15% for Ps groups and 11% and 18% for Ns groups, respectively. Additionally, PVP exhibited higher conductivity and transparency, making it suitable and having a good affinity for developing films of high-quality [47, 63]. Moreover, the incorporation of GO demonstrated a noteworthy impact on the adjustable bandgap [64]. As a result, there was a significant decrease in the energy gap values of the nanocomposites, as shown in Figs. 9 and 10. This information is also presented in Table 3, indicating that the occurrence of the C-O group in PVP reduced the energy gap values of the Ps group. In contrast, those of the Ns group were lower through the existence of the O–H group. However, in both groups, there was an enhancement in the results attributed to the addition of CS and GO.

In summary, in the optical results, the optical absorption edge was red-shifted towards higher wavelength and lower energy after adding CS and GO to P1 and N1 samples. Therefore, the absorbance was increased, and the transmittance was decreased. The direct and indirect optical energy gap was also reduced.

Figures 11 and 12 exhibited the antibacterial activity of the samples. The investigation involved testing against Gram-negative and -positive bacterial strains that were assessed using the agar well diffusion procedure [65, 66]. Roughly 20 ml of Muller-Hinton agar (MH) were aseptically dispensed into sterile Petri dishes. A sterile wire loop was used from their respective stock cultures to get bacterial strains [67]. Following the organism's cultivation, using a sterile tip, 6 mm-diameter wells were created on the agar plates—equal concentrations of Ps and Ns samples were added to the wells. At 37°C, the plates containing the Ps and Ns samples and the test organisms were left to incubate overnight. After that, the average diameter of the inhibition zones was calculated [68, 69]. The activity of both P1 and N1 against *S. aureus* was low; this finding of these polymers, independent or mixed, was reported by several studies [70–72]. At the same time, it started to improve to 11 and 14 mm of P3 and N3 after the contribution of CS and GO, as shown in Fig. 11. In Fig. 12, strong activity against *E. coli* was revealed, and it improved from 18 to 20 and 19 to 23 mm, respectively. All results of antibacterial activity with different concentrations are shown in the figures below, and all details are revealed in Table 4.

These results matched other results when the same polymers with different nanomaterials. [4, 6, 70, 72, 73].

**Table 3** Condensed the optical energy gap for P1, P2, P3, and N1, N2, N3 nanocomposites

| Indirect transition (eV) | | |
|---|---|---|
| **Samples** | **Allowed** | **Forbidden** |
| **P1** | 3.45 | 3.4 |
| **P2** | 3.3 | 3.25 |
| **P3** | 3.05 | 2.95 |
| **N1** | 4.05 | 3.9 |
| **N2** | 3.9 | 3.55 |
| **N3** | 3.65 | 3.2 |

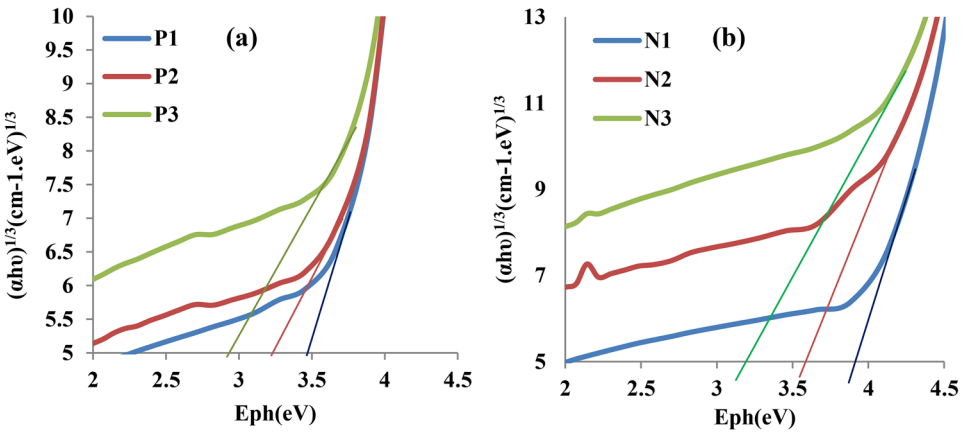


**Fig. 10** Energy gap for the forbidden indirect transition concerning photon energy **a** Ps, and **b** Ns

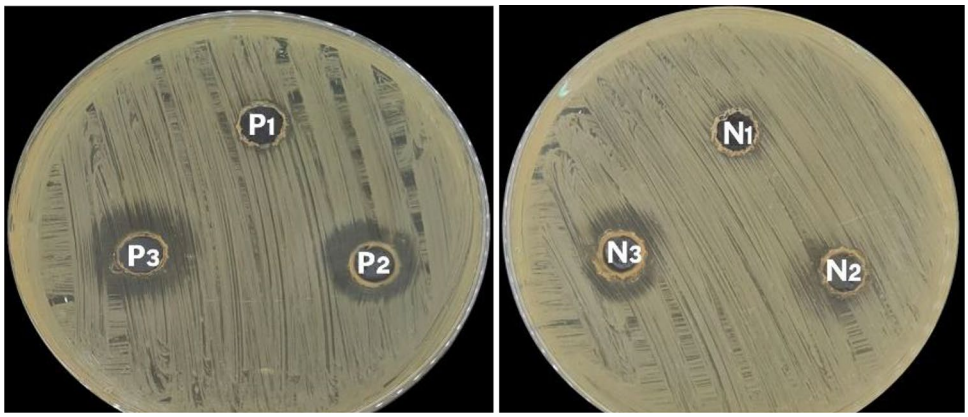


**Fig. 11** Antibacterial activity of samples against *S. aureus*.

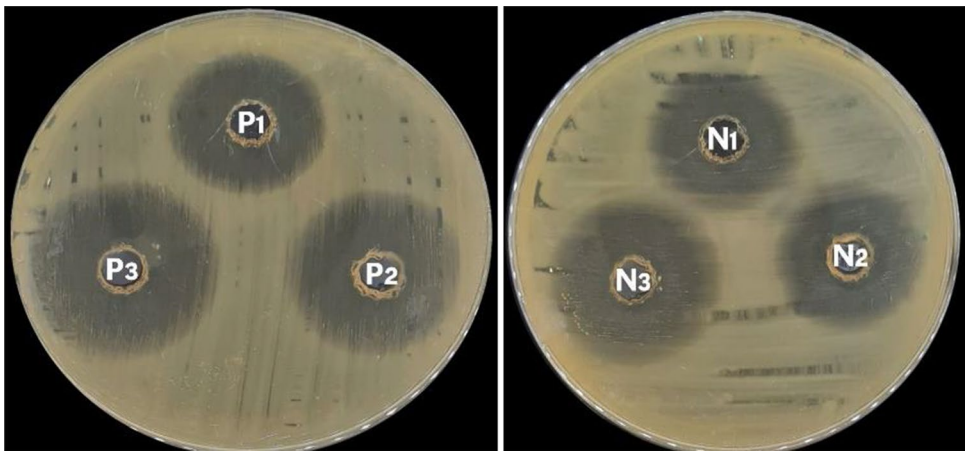


**Fig. 12** Antibacterial activity of samples against *E. Coli*.

**Table 4** Explain the antibacterial activity of nanoparticles

| Sample | Antibacterial analysis (Zone of inhibition (mm)) | | |
|---|---|---|---|
| ***S. aureus*** | P1 | P2 | P3 |
| | 0 | 12 | 14 |
| ***E. coli*** | P1 | P2 | P3 |
| | 19 | 21 | 23 |
| ***S. aureus*** | N1 | N2 | N3 |
| | 0 | 9 | 11 |
| ***E. coli*** | N1 | N2 | N3 |
| | 18 | 19 | 20 |

## Conclusions

The following procedure succeeded in fabricating new nanocomposites that consist of polyvinyl alcohol (PVA)/polyacrylic acid (PAA)/chitosan (CS) and graphene oxide (GO). It, compared with other nanocomposites, has polymers from the same family but with different functional groups, polyvinyl pyrrolidone (PVP)/polyacrylic acid (PAA)/chitosan (CS)/graphene oxide (GO) (Ps). The results of FTIR and XRD showed a clear and strong correlation in terms of optical characteristics; an

improvement in the energy gap up to 15% of Ps and 18% of Ns groups was noticed. The optical features of P3 communications presented the lowest energy gap compared with N3. Additionally, the antibacterial activity of P3 also presented better inhabitation of the zone than N3 samples. Generally, both samples revealed better activity in killing *E. coli* than *S. aureus*. Interestingly, samples including polyvinyl pyrrolidone showed better results than samples containing polyvinyl alcohol. These results exposed a promising combination of nanotechnology in optoelectronic devices, biology, and medicine to find new antimicrobial materials that could be utilized for biological sensors, coating medicine toles, and other biological applications.

**Acknowledgements** Sarah Sabah Aljelawy gratefully acknowledges the University of Babylon, College of Education for pure science, Iraq.

**Author contributions** Sarah Sabah Aljelawy responds to conceptualization, investigation, acquisition, software, formal analysis, data curation, writing – original draft, and Funding. Ehssan Al-Bermany and Ali Razzaq Abdulridha supervise, validate, review, and edit project administration, investigation, and resources.

**Funding** Not applicable.

**Data availability** The data are available in the manuscript.

## Declarations

**Ethical approval** Not applicable.

**Competing interests** Not applicable.

**Consent to participate** Not applicable.

**Consent for publication** Not applicable.

**Declaration of generative AI in scientific writing** Not applicable.

## References

1. El Sayed AM, El-Gamal S (2015) Synthesis and investigation of the electrical and dielectric properties of Co3O4/(CMC+PVA) nanocomposite films. J Polym Res 22:97. https://doi.org/10.1007/s10965-015-0732-4
2. Alawi AI, Al-Bermany E (2023) Newly Fabricated Ternary PAAm-PVA-PVP Blend Polymer Doped by SiO2: Absorption and Dielectric Characteristics for Solar Cell Applications and Antibacterial Activity. SILICON 15:5773–5789. https://doi.org/10.1007/s12633-023-02477-5
3. Al Mogbel MS, Elabbasy MT, Mohamed RS et al (2021) Improvement in antibacterial activity of Poly Vinyl Pyrrolidone/Chitosan incorporated by graphene oxide NPs via laser ablation. J Polym Res 28:1–8. https://doi.org/10.1007/s10965-021-02838-x
4. Abdali K, Abass KH, Al-Bermany E et al (2022) Morphological, Optical, Electrical Characterizations and Anti- Escherichia coli Bacterial Efficiency (AECBE) of PVA/PAAm/PEO Polymer Blend Doped with Silver NPs. Nano Biomed Eng 14:114–122. https://doi.org/10.5101/nbe.v14i2.p114-122
5. Whiteley KS, Heggs TG, Koch H et al (2000) Polyolefins. In: Ullmann's Encyclopedia of Industrial Chemistry. Wiley-VCH Verlag GmbH & Co. KGaA, Weinheim, Germany
6. Abdali K, Rabee BH, Al-Bermany E et al (2023) Effect of Doping Sb2O3 NPs on Morphological, Mechanical, and Dielectric Properties of PVA/PVP Blend Film for Electromechanical Applications. NANO 18:2350011. https://doi.org/10.1142/S179329202350011X
7. Kadhim MA, Al-Bermany E (2020) Enhance the electrical properties of the novel fabricated pmma-pva/ graphene based nanocomposites. J Green Eng 10:3465–3483
8. Badawi A, Alsufyani SJ, Alharthi SS et al (2022) Impact of gamma irradiation on the structural, linear and nonlinear optical properties of lead oxide incorporated PVA/graphene blend for shielding applications. Opt Mater 127:112244. https://doi.org/10.1016/j.optmat.2022.112244
9. Rashid A-KJ, Jawad ED, Kadem BY (2011) A Study of Some Mechanical Properties of Iraqi Palm Fiber-PVA Composite by Ultrasonic. Eur J Sci Res 61:203–209
10. Sudheesh P, Sharafudeen KN, Vijayakumar S, Chandrasekharan K (2011) Preparation and study of nonlinear optical response of Ag and Au nano particles doped PVA/PVP thin films. J Opt 40:193–197. https://doi.org/10.1007/s12596-011-0053-x
11. Billmeyer FW (1963) Textbook of Polymer Science. Kobunshi 12:240–251. https://doi.org/10.1295/kobunshi.12.240
12. Al-shammari AK, Al-Bermany E, Al-Bermany E (2021) New Fabricated (PAA-PVA/GO) and (PAAm-PVA/GO) Nanocomposites: Functional Groups and Graphene Nanosheets effect on the Morphology and Mechanical Properties. J Phys Conf Ser 1973. https://doi.org/10.1088/1742-6596/1973/1/012165
13. Elashmawi IS, Menazea AA (2022) Dual laser ablation process assisted the synthesis of titanium dioxide and graphene oxide nanoparticles embedded in chitosan for electrical applications. Opt Mater (Amst) 134:1–5. https://doi.org/10.1016/j.optmat.2022.113177
14. Bhardwaj N, Kundu SC (2010) Electrospinning: A fascinating fiber fabrication technique. Biotechnol Adv 28:325–347
15. Subramanian A, Vu D, Larsen GF, Lin HY (2005) Preparation and evaluation of the electrospun chitosan/PEO fibers for potential applications in cartilage tissue engineering. J Biomater Sci Polym Ed 16:861–873. https://doi.org/10.1163/1568562054255682
16. Bhattarai N, Edmondson D, Veiseh O et al (2005) Electrospun chitosan-based nanofibers and their cellular compatibility. Biomaterials 26:6176–6184. https://doi.org/10.1016/j.biomaterials.2005.03.027
17. Al-Bermany E, Qais D, Al-Rubaye S (2019) Graphene effect on the mechanical properties of poly (ethylene oxide)/ graphene oxide nanocomposites using ultrasound technique. J Phys Conf Ser 1234:012011. https://doi.org/10.1088/1742-6596/1234/1/012011
18. Li S, Wang D, Wang Z et al (2015) Laser-induced fabrication of single crystal zinc hydroxyl dodecylsulfate nano-sheets with excellent fluorescence emission. RSC Adv 5:63233–63239. https://doi.org/10.1039/c5ra11191a
19. Cao T, Zhao F, Da Z et al (2016) A novel graphene oxide-polyimide as optical waveguide material: Synthesis and thermo-optic switch properties. Opt Mater (Amst) 60:45–49. https://doi.org/10.1016/j.optmat.2016.07.001
20. Hummers WS, Offeman RE (1958) Preparation of Graphitic Oxide. J Am Chem Soc 80:1339–1339. https://doi.org/10.1021/ja01539a017
21. Al-shammari AK, Al-Bermany E, Al-Bermany E (2022) Polymer functional group impact on the thermo-mechanical properties of polyacrylic acid, polyacrylic amide- poly (vinyl alcohol) nanocomposites reinforced by graphene oxide nanosheets. J Polym Res 29:351. https://doi.org/10.1007/s10965-022-03210-3
22. Yao N, Li C, Yu J et al (2020) Insight into adsorption of combined antibiotic-heavy metal contaminants on graphene oxide in water.

Sep Purif Technol 236:116278. https://doi.org/10.1016/j.seppur.2019.116278
23. World Health Organization (2014) Antimicrobial resistance - global report on surveillance. World Heal Organ 61:383–394
24. Lofrano G, Carotenuto M, Libralato G et al (2016) Polymer functionalized nanocomposites for metals removal from water and wastewater: An overview. Water Res 92:22–37
25. Abou-Taleb MH (2009) Thermal and spectroscopic studies of poly(n-vinyl pyrrolidone)/poly(vinyl alcohol) blend films. J Appl Polym Sci 114:1202–1207. https://doi.org/10.1002/app.30082
26. Hatta FF, Yahya MZA, Ali AMM et al (2005) Electrical conductivity studies on PVA/PVP-KOH alkaline solid polymer blend electrolyte. Ionics (Kiel) 11:418–422. https://doi.org/10.1007/BF02430259
27. Abdali K, Al-Bermany E, Abass KH et al (2023) Impact the silver nanoparticles on properties of new fabricated polyvinyl alcohol-polyacrylamide- polyacrylic acid nanocomposites films for optoelectronics and radiation pollution applications. J Polym Res 30:1–9. https://doi.org/10.1007/s10965-023-03514-y
28. Alharthi SS, Badawi A (2024) Effect of Ag/CuS nanoparticles loading to enhance linear/nonlinear spectroscopic and electrical characteristics of PVP/PVA blends for flexible optoelectronics. J Vinyl Addit Technol 30:230–243. https://doi.org/10.1002/vnl.22044
29. Yang M, Wang Z, Li M et al (2023) The synthesis, mechanisms, and additives for bio-compatible polyvinyl alcohol hydrogels: A review on current advances, trends, and future outlook. J Vinyl Addit Technol 29:939–959. https://doi.org/10.1002/vnl.21962
30. Heiba ZK, Mohamed MB, Ahmed SI, Alhazime AA (2021) Tailoring the optical properties of PVA/PVP blend by doping with Cu/MnS nanoparticles. J Vinyl Addit Technol 27:410–418. https://doi.org/10.1002/vnl.21815
31. Al-Bermany E, Chen B (2021) Preparation and characterisation of poly(ethylene glycol)-adsorbed graphene oxide nanosheets. Polym Int 70:341–351. https://doi.org/10.1002/pi.6140
32. Alawi AI, Al-Bermany E, Alnayli RS et al (2024) Impact of SiO2–GO hybrid nanomaterials on opto-electronic behavior for novel glass quinary (PAAm–PVP–PVA/SiO2–GO) hybrid nanocomposite for antibacterial activity and shielding applications. Opt Quantum Electron 56:429. https://doi.org/10.1007/s11082-023-06070-3
33. Mohammed R, Jawad H, Al-Zubiedy A (2021) Blended PVA/PVP electro spun nanofibers for coating application. J Phys Conf Ser 2114:012031. https://doi.org/10.1088/1742-6596/2114/1/012031
34. Ibrahim M, Mahmoud AA, Osman O et al (2010) Molecular spectroscopic analysis of nano-chitosan blend as biosensor. Spectrochim Acta - Part A Mol Biomol Spectrosc 77:802–806. https://doi.org/10.1016/j.saa.2010.08.007
35. Moharram MA, Khafagi MG (2007) Application of FTIR spectroscopy for structural characterization of ternary poly (acrylic acid)–metal–poly (vinyl pyrrolidone) complexes. J Appl Polym Sci 105:1888–1893
36. Manavi-Tehrani I, Rabiee M, Parviz M et al (2010) Preparation, characterization and controlled release investigation of biocompatible pH-sensitive PVA/PAA hydrogels. Macromol Symp 296:457–465. https://doi.org/10.1002/masy.201051062
37. Kim DS, Park HB, Rhim JW, Lee YM (2005) Proton conductivity and methanol transport behavior of cross-linked PVA/PAA/silica hybrid membranes. Solid State Ionics 176:117–126
38. Kim J, Kang T, Kim H et al (2019) Preparation of PVA/PAA nanofibers containing thiol-modified silica particles by electrospinning as an eco-friendly Cu (II) adsorbent. J Ind Eng Chem 77:273–279
39. Shah S, Pandey OP, Mohammed J et al (2020) Reduced graphene oxide (RGO) induced modification of optical and magnetic properties of M-type nickel doped barium hexaferrite. J Sol-Gel Sci Technol 93:579–586. https://doi.org/10.1007/s10971-019-05210-0
40. Jin S, Liu M, Chen S, Gao C (2010) A drug-loaded gel based on polyelectrolyte complexes of poly (acrylic acid) with poly (vinylpyrrolidone) and chitosan. Mater Chem Phys 123:463–470
41. Salam MA, Alsultany FH, Al-Bermany E et al (2024) Impact of graphene oxide nanosheets and polymethyl methacrylate on nano/hybrid-based restoration dental filler composites: ultrasound behavior and antibacterial activity. J Ultrasound null:null. https://doi.org/10.1007/s40477-023-00855-8
42. Rashed ER, Abd El-Rehim HA, El-Ghazaly MA (2015) Potential efficacy of dopamine loaded-PVP/PAA nanogel in experimental models of Parkinsonism: Possible disease modifying activity. J Biomed Mater Res Part A 103:1713–1720
43. Al-Abbas SS, Ghazi RA, Al-Bermany E et al (2023) Structure and absorption behaviour of PAAm-PVA-based nanocomposites reinforced using graphene. 2ND Int Conf Math Appl Sci Inf Commun Technol null:null. https://doi.org/10.1063/5.0161591
44. Arik N, Inan A, Ibis F et al (2019) Modification of electrospun PVA/PAA scaffolds by cold atmospheric plasma: Alignment, antibacterial activity, and biocompatibility. Polym Bull 76:797–812
45. Cheng Y, Hu Y, Xu M et al (2020) High strength polyvinyl alcohol/polyacrylic acid (PVA/PAA) hydrogel fabricated by Cold-Drawn method for cartilage tissue substitutes. J Biomater Sci Polym Ed 31:1836–1851
46. Wu Y-T, Yu Y-H, Nguyen V-H, Wu JCS (2015) In-situ FTIR spectroscopic study of the mechanism of photocatalytic reduction of NO with methane over Pt/TiO2 photocatalysts. Res Chem Intermed 41:2153–2164. https://doi.org/10.1007/s11164-013-1337-3
47. Lilleby Helberg RM, Dai Z, Ansaloni L, Deng L (2020) PVA/PVP blend polymer matrix for hosting carriers in facilitated transport membranes: Synergistic enhancement of CO2 separation performance. Green Energy Environ 5:59–68. https://doi.org/10.1016/j.gee.2019.10.001
48. Al-Abbas SS, Ghazi RA, Al-shammari AK et al (2021) Influence of the polymer molecular weights on the electrical properties of Poly(vinyl alcohol) – Poly(ethylene glycols)/Graphene oxide nanocomposites. Mater Today Proc 42:2469–2474. https://doi.org/10.1016/j.matpr.2020.12.565
49. Siburian R, Sihotang H, Lumban Raja S et al (2018) New route to synthesize of graphene nano sheets. Orient J Chem 34:182–187. https://doi.org/10.13005/ojc/340120
50. Johra FT, Lee JW, Jung WG (2014) Facile and safe graphene preparation on solution based platform. J Ind Eng Chem 20:2883–2887. https://doi.org/10.1016/j.jiec.2013.11.022
51. Gupta S, Pramanik AK, Kailath A et al (2009) Composition dependent structural modulations in transparent poly(vinyl alcohol) hydrogels. Colloids Surfaces B Biointerfaces 74:186–190. https://doi.org/10.1016/j.colsurfb.2009.07.015
52. Ricciardi R, Auriemma F, De Rosa C, Lauprêtre F (2004) X-ray Diffraction Analysis of Poly(vinyl alcohol) Hydrogels, Obtained by Freezing and Thawing Techniques. Macromolecules 37:1921–1927. https://doi.org/10.1021/ma035663q
53. Rogina A, Ivanković M, Ivanković H (2013) Preparation and characterization of nano-hydroxyapatite within chitosan matrix. Mater Sci Eng C 33:4539–4544. https://doi.org/10.1016/j.msec.2013.07.008
54. Ghazi RA, Al-Mayalee KH, Al-Bermany E et al (2022) Impact of polymer molecular weights and graphene nanosheets on fabricated PVA-PEG/GO nanocomposites: Morphology, sorption behavior and shielding application. AIMS Mater Sci 9:584–603. https://doi.org/10.3934/matersci.2022035
55. Al-Bermany E, Chen B (2023) Effect of the Functional Groups of Polymers on Their Adsorption Behavior on Graphene Oxide Nanosheets. Macromol Chem Phys 224:1–10. https://doi.org/10.1002/macp.202300101

56. Indolia AP, Gaur MS (2013) Optical properties of solution grown PVDF-ZnO nanocomposite thin films. J Polym Res 20:1–8. https://doi.org/10.1007/s10965-012-0043-y
57. Chang H, Wu H (2013) Graphene-based nanocomposites: preparation, functionalization, and energy and environmental applications. Energy Environ Sci 6:3483. https://doi.org/10.1039/c3ee42518e
58. Search H, Journals C, Contact A et al (2014) Optical, dielectric and electrical properties of PVA doped with Sn nanoparticles. Mater Res Express 1:1–10. https://doi.org/10.1088/2053-1591/1/2/025024
59. Feng Y, Dong N, Wang G et al (2015) Saturable absorption behavior of free-standing graphene polymer composite films over broad wavelength and time ranges. Opt Express 23:666–669. https://doi.org/10.1364/OE.23.000559
60. Barroso-Bujans F, Fernandez-Alonso F, Cerveny S et al (2012) Two-Dimensional Subnanometer Confinement of Ethylene Glycol and Poly(ethylene oxide) by Neutron Spectroscopy: Molecular Size Effects. Macromolecules 45:3137–3144. https://doi.org/10.1021/ma202655f
61. Abdelamir AI, Al-Bermany E, Sh Hashim F (2019) Enhance the Optical Properties of the Synthesis PEG/Graphene- Based Nanocomposite films using GO nanosheets. J Phys Conf Ser 1294:022029. https://doi.org/10.1088/1742-6596/1294/2/022029
62. Tauc J (1970) Absorption edge and internal electric fields in amorphous semiconductors. Mater Res Bull 5:721–729. https://doi.org/10.1016/0025-5408(70)90112-1
63. Aziz SB, Rasheed MA, Hussein AM, Ahmed HM (2017) Fabrication of polymer blend composites based on [PVA-PVP] (1–x):(Ag 2 S) x (0.01 ≤ x ≤ 0.03) with small optical band gaps: Structural and optical properties. Mater Sci Semicond Process 71:197–203. https://doi.org/10.1016/j.mssp.2017.05.035
64. Aldulaimi NR, Al-Bermany E (2022) Tuning the bandgap and absorption behaviour of the newly-fabricated ultrahigh molecular weight polyethylene oxide- polyvinyl alcohol/ graphene oxide hybrid nanocomposites. Polym Polym Compos 30:096739112211121. https://doi.org/10.1177/09673911221112196
65. Bahjat HH, Ismail RA, Sulaiman GM, Jabir MS (2021) Magnetic Field-Assisted Laser Ablation of Titanium Dioxide Nanoparticles in Water for Anti-Bacterial Applications. J Inorg Organomet Polym Mater 31:3649–3656. https://doi.org/10.1007/s10904-021-01973-8
66. Khashan KS, Abdulameer FA, Jabir MS et al (2020) Anticancer activity and toxicity of carbon nanoparticles produced by pulsed laser ablation of graphite in water. Adv Nat Sci Nanosci Nanotechnol 11:035010. https://doi.org/10.1088/2043-6254/aba1de
67. Jaber GS, Khashan KS, Abbas MJ (2021) Study the antibacterial activity of zinc oxide nanoparticles synthesis by laser ablation in liquid. Mater Today Proc 42:2668–2673. https://doi.org/10.1016/j.matpr.2020.12.646
68. Jihad MA, Noori FTM, Jabir MS et al (2021) Polyethylene Glycol Functionalized Graphene Oxide Nanoparticles Loaded with Nigella sativa Extract: A Smart Antibacterial Therapeutic Drug Delivery System. Molecules 26:3067. https://doi.org/10.3390/molecules26113067
69. Mohammed MKA, Mohammad MR, Jabir MS, Ahmed DS (2020) Functionalization, characterization, and antibacterial activity of single wall and multi wall carbon nanotubes. IOP Conf Ser Mater Sci Eng 757:012028. https://doi.org/10.1088/1757-899X/757/1/012028
70. Shahrousvand M, Mirmasoudi SS, Pourmohammadi-Bejarpasi Z, et al (2023) Polyacrylic acid/ polyvinylpyrrolidone hydrogel wound dressing containing zinc oxide nanoparticles promote wound healing in a rat model of excision injury. Heliyon 9:e19230. https://doi.org/10.1016/j.heliyon.2023.e19230
71. Santiago-Morales J, Amariei G, Letón P, Rosal R (2016) Antimicrobial activity of poly(vinyl alcohol)-poly(acrylic acid) electrospun nanofibers. Colloids Surfaces B Biointerfaces 146:144–151. https://doi.org/10.1016/j.colsurfb.2016.04.052
72. Albalwi H, Abou El Fadl FI, Ibrahim MM, Abou Taleb MF (2022) Antibacterial impact of acrylic acid /polyvinyl alcohol/ MgO various nanocomposite hydrogels prepared by gamma radiation. Polym Bull 79:7697–7709. https://doi.org/10.1007/s00289-021-03866-9
73. Abd El-Kader MFH, Elabbasy MT, Ahmed MK, Menazea AA (2021) Structural, morphological features, and antibacterial behavior of PVA/PVP polymeric blends doped with silver nanoparticles via pulsed laser ablation. J Mater Res Technol 13:291–300. https://doi.org/10.1016/j.jmrt.2021.04.055